NEUROSCIENCE

ATP1A3 as a target for isolating neuron-specific extracellular vesicles from human brain and biofluids

Yang You[1,2]†, Zhengrong Zhang[1]†, Nadia Sultana[3,4], Maria Ericsson[5], Yuka A. Martens[1], Min Sun[6], Takahisa Kanekiyo[1], Seiko Ikezu[1,2], Scott A. Shaffer[3,4], Tsuneya Ikezu[1,2]*

Neuron-derived extracellular vesicles (NDEVs) are potential biomarkers of neurological diseases although their reliable molecular target is not well established. Here, we demonstrate that ATPase Na^+/K^+ transporting subunit alpha 3 (ATP1A3) is abundantly expressed in extracellular vesicles (EVs) isolated from induced human neuron, brain, cerebrospinal fluid, and plasma in comparison with the presumed NDEV markers NCAM1 and L1CAM by using super-resolution microscopy and biochemical assessments. Proteomic analysis of immunoprecipitated $ATP1A3^+$ brain-derived EVs shows higher enrichment of synaptic markers and cargo proteins relevant to Alzheimer's disease (AD) compared to $NCAM1^+$ or $LICAM^+$ EVs. Single particle analysis shows the elevated amyloid-β positivity in $ATP1A3^+$ EVs from AD plasma, providing better diagnostic prediction of AD over other plasma biomarkers. Thus, ATP1A3 is a reliable target to isolate NDEV from biofluids for diagnostic research.

INTRODUCTION

Extracellular vesicles (EVs) are cell-derived small membranous vesicles carrying a large diversity of molecules including lipids, nucleic acids, and proteins (*1*). EV cargos could be dynamically altered under the pathophysiological conditions and reflect a disease-specific signature. Therefore, they are a promising source for understanding the state of brain and discovering biomarkers of neurological disorders. Over the past several years, there has been a keen interest in capturing neuron-specific EVs from patient-derived biopsies or biofluids and characterizing their contents as a pathological reflection of the central nervous system (CNS). Most studies attempted to enrich putative neuron-derived EVs (NDEVs) by immunocapturing a presumed neural marker L1 cell adhesion molecule (L1CAM) (*2*). Although this approach has identified L1CAM-associated biomarker signatures that correlate with neurodegenerative and psychiatric diseases, the reliability of using L1CAM as a marker of brain neuronal EVs has been questioned (*3*). Therefore, more reliable reproducible NDEV markers are needed to isolate and characterize bona fide NDEVs from human samples.

Our recent study characterized proteomic profiles of EVs from four human neural cell types, excitatory neurons, astrocytes, microglia-like cells, and oligodendrocytes, and identified adenosine triphosphatase (ATPase) Na^+/K^+ transporting subunit alpha 3 (ATP1A3) as one of the abundant neuron-specific EV markers (*4*). ATP1A3 is α-3 catalytic subunit of the neuronal Na^+/K^+ ATPase, an integral membrane protein regulating the electrochemical gradients of Na^+ and K^+ ions (*5*). Unlike L1CAM, which is widely expressed in both CNS and periphery, ATP1A3 is mostly enriched in brains with some specific expression in heart muscles according to the Human Protein Atlas database (https://proteinatlas.org/). Single-cell RNA sequencing analysis of human cerebral cortex further shows enrichment of *ATP1A3* in excitatory and inhibitory neurons (*6*), suggesting the neuronal origin of *ATP1A3*. Here, we conduct both single and bulk EV analyses to evaluate whether ATP1A3 is specific to NDEVs and a promising target for NDEV pulldown from accessible biofluids for disease monitoring. The two proposed NDEV markers L1CAM and neural cell adhesion molecule 1 (NCAM1) (*7*) were also evaluated for the comparisons.

RESULTS

ATP1A3 is a neuron-specific protein and associated with EVs in human brain tissues and biofluids

Immunofluorescent staining of ATP1A3 in adult mouse brain revealed the abundant expression of its protein across different brain regions including cortex, hippocampus, striatum, and thalamus (fig. S1A). To investigate the cell type–specific expression of ATP1A3, colocalization analysis was conducted between ATP1A3 and specific cell markers, including neurons ($MAP2^+$), astrocytes ($GFAP^+$), and microglia ($IBA1^+$), in the hippocampal area of both wild-type and Alzheimer's disease (AD) mouse model ($APP^{NL\text{-}G\text{-}F}$; fig. S1B). In addition, similar analysis was performed using human brain tissues obtained from healthy individual and AD patient (fig. S1C). Our data showed a higher degree of overlap in fluorescence intensity and distribution between ATP1A3 and the neuronal marker MAP2, as compared to glial fibrillar acidic protein (GFAP) and ionized calcium-binding adapter molecule 1 (IBA1) staining, in all experimental conditions. These results strongly suggest that ATP1A3 expression is predominantly specific to neurons. Moreover, RNA expression data accessed from the Human Protein Atlas database further support our observation, demonstrating a more confined expression pattern of ATP1A3 in the brain with a notable enrichment in neurons than NCAM1 and L1CAM (fig. S2).

As ATP1A3 is a multiple transmembrane protein expressed on neurons, we expected that it is also associated with EVs on their surface. We therefore isolated EVs derived from human induced pluripotent stem cell–derived excitatory neurons (iNeurons),

[1]Department of Neuroscience, Mayo Clinic, Jacksonville, FL, USA. [2]Department of Pharmacology and Experimental Therapeutics, Boston University School of Medicine, Boston, MA, USA. [3]Department of Biochemistry and Molecular Biotechnology, University of Massachusetts Chan Medical School, Worcester, MA, USA. [4]Mass Spectrometry Facility, University of Massachusetts Chan Medical School, Shrewsbury, MA USA. [5]Department of Cell Biology, Harvard Medical School, Boston, MA, USA. [6]Nanoview Biosciences, Boston, MA, USA School, Boston, MA, USA.
*Corresponding author. Email: ikezu.tsuneya@mayo.edu
†These authors contributed equally to this work.

human brain tissues, cerebrospinal fluid (CSF), and plasma and characterized the presence of molecules of interest using four complementary techniques (Fig. 1A). Our iNeuron differentiation by overexpressing the neuronal transcriptional factor neurogenin-2 (NGN2) after puromycin selection of transduced cells (*8*) resulted in over 97% MAP2$^+$ neuronal cells with less contamination of GFAP$^+$ astrocytes (fig. S3, A and B). The high purity of the culture was also supported by our previously published proteomics dataset (*4*), showing a remarkable enrichment of neuron-specific proteins including MAP2, MAPT, and synaptic proteins in iNeurons (fig. S3C). In addition, the NDEV marker candidates including ATP1A3, NCAM1, and L1CAM were also detected (fig. S3D). Next, we applied immuno-electron microscopy to confirm the presence of ATP1A3, NCAM1, and L1CAM on the EV surface by labeling with 5-nm gold particles for these markers and 10-nm gold particles for CD9. The immuno-labeling of CD9 was detectable in iNeuron-, brain-, CSF-, and plasma-EVs (Fig. 1B, left column). Double immunostaining showed that ATP1A3, NCAM1, or L1CAM was detected with CD9 in a single EV in all of these samples (Fig. 1B, second to fourth columns).

We next used single-particle interferometric reflectance imaging sensor (SP-IRIS) analysis (*9*) to determine the population of these NDEV markers in different EV preparations after EV affinity binding to tetraspanins on Exoview chips (fig. S4A). Total fluorescent particles in each spot preconjugated with anti-CD9, anti-CD81, anti-CD63, and isotype control immunoglobulin G (IgG) antibodies were counted in EV samples, revealing the different tetraspanin subpopulations between iNeuron-, brain-, and CSF-EVs (fig. S4, B and C). Analysis of the fluorescent expression of NDEV markers confirmed the presence of ATP1A3, NCAM1, and L1CAM in those EV preparations and revealed their colocalizations with pan-tetraspanins. The captured iNeuron-EVs displayed a higher level of ATP1A3 compared to NCAM1 and L1CAM, particularly in CD9 captured spots (Fig. 1, C and D). Intriguingly, we observed the higher percentage of NCAM1$^+$ particles in CD9 and CD81 captured spots from brain-EV, while ATP1A3$^+$ particles were more enriched in CD63 captured spots from brain- and CSF-EV (Fig. 1, E and F). The colocalization analysis showed diverse EV subpopulations (e.g., pan-tetraspanins$^+$ EVs, ATP1A3$^+$ EVs, NCAM1$^+$ EVs, L1CAM$^+$ EVs, ATP1A3$^+$ NCAM1$^+$ EVs, ATP1A3$^+$ L1CAM$^+$ EVs, etc.) in brain- and CSF-EVs (fig. S4D), suggesting the heterogeneity of neuronal EVs in human samples.

Single- and bulk-EV analysis demonstrated the higher enrichment of ATP1A3 associated EVs than NCAM1 and L1CAM in human samples

To confirm the expression and colocalization of surface markers in four EV preparations, we performed super-resolution imaging of single EVs captured by EV profiler kit [Oxford Nanoimager (ONI)] and stained with fluorescent antibodies against pan-tetraspanins (CD9/CD81/CD63) and neuronal EV markers (ATP1A3, NCAM1, and L1CAM) at a single vesicle resolution by direct stochastic optical reconstruction microscopy (dSTORM) (Fig. 2A) (*10*). The clustering analysis showed a higher percentage of ATP1A3$^+$ EV subpopulation when compared to NCAM1 in iNeuron-EV (35.7 versus 0.0%), CSF-EV (56.8 versus 0.5%), and plasma-EV (11.4 versus 0.9%), while fewer ATP1A3$^+$ EV population was identified compared to NCAM1 in brain-EV (12.5 versus 33.1%; Fig. 2, B and C). Similarly, we can detect greater ATP1A3$^+$ EV subpopulation with respect to L1CAM in iNeuron-EV (20.4 versus 0.1%), brain-EV (19.4 versus 4.5%), CSF-EV (29.7 versus 0.9%), and plasma-EV (8.1 versus 0.2%; Fig. 2, D to F). Thus, our data demonstrated that those three candidate markers were present on the surface of EVs isolated from iNeurons, brain, CSF, and plasma and that the ATP1A3$^+$ EVs is more reliably detectable in these human biospecimens than NCAM1$^+$ and L1CAM$^+$ EVs by dSTORM techniques.

Next, we biochemically characterized EVs from brain, CSF, and plasma samples. Immunoblotting confirmed the expression of EV specific markers (CD9 and CD81) and the absence of non-EV markers [GM130, cytochrome C (CytoC), and H2A] in brain-EV (fig. S5A). Notably, ATP1A3 showed significantly higher enrichment in EV fractions compared to brain lysates, while we did not observe such enrichment with NCAM1 and L1CAM (fig. S5B). In CSF and plasma samples, ATP1A3 was also highly enriched in EV fractions although both NCAM1 and L1CAM were rather depleted in EVs (fig. S6, A and B). To determine whether those three NDEV markers were expressed on the EV surface, we performed proteinase treatment assay (fig. S7A). Proteinase K treatment significantly diminished the amount of ATP1A3, NCAM1, L1CAM, and CD81 in brain-EVs compared to microtubule associated protein tau (Tau) and glyceraldehyde phosphate dehydrogenase (GAPDH), which were intraluminal proteins of EVs (fig. S7, B and C) (*11*, *12*). These biochemical evaluations ensure that ATP1A3 is associated with neuronal EV surface and enriched in human brain-, CSF-, and plasma- EV samples compared to NCAM1 and L1CAM.

ATP1A3$^+$ EV immunoprecipitated from human brain tissues displays higher neuronal cell type specificity over NCAM1$^+$ and L1CAM$^+$ EVs by label-free mass spectrometry

EV cargo molecules can reflect the physiological or disease status of the cells of origin (*13*). To characterize the signature of cargo molecules in three different NDEVs, we performed proteomic analysis of ATP1A3, L1CAM, or NCAM1-associated brain-EVs separated by affinity capture method (Fig. 3A). First, we examined markers for EV, synapse, and glia in ATP1A3$^+$, NCAM1$^+$, or L1CAM$^+$ EV immunocaptured from the equal amount of brain-EVs by immunoblotting (Fig. 3B). The common EV markers (e.g., FLOT1, CD81, and CD9) were present in all the immunoprecipitated EV samples (Fig. 3B). We observed a better enrichment of neuron-specific proteins including Tau, synaptophysin (SYP), and synaptosome-associated protein 25 (SNAP25) by ATP1A3 and NCAM1 immunoprecipitation than L1CAM (Fig. 3B). In addition, the presumed glia makers (microglial TMEM119 and astrocytic GFAP) were undetectable in these immunoprecipitated NDEVs. Label-free liquid chromatography–mass spectrometry analysis of ATP1A3$^+$, NCAM1$^+$, and L1CAM$^+$ brain-EVs (table S1) identified a total of 318 proteins in ATP1A3$^+$ EVs, 275 proteins in NCAM1$^+$ EVs, and 131 proteins in L1CAM$^+$ EVs after the exclusion of non-specific proteins coimmunoprecipitated by isotype control IgG (Fig. 3, C and D). The heatmap displayed the clustering of total 507 identified EV protein, which showed neuronal markers (ATP1A3, NCAM1, and L1CAM), common EV markers (e.g., CD9 and CD81), and neuron-specific molecules [e.g., SYP, SNAP25, and neuroplastin (NPTN)] (fig. S8A). Among the 249 overlapping proteins between ATP1A3$^+$ and NCAM1$^+$ EVs, we ranked the differentially expressed proteins (DEPs) based on the fold change in protein abundance and determined a higher

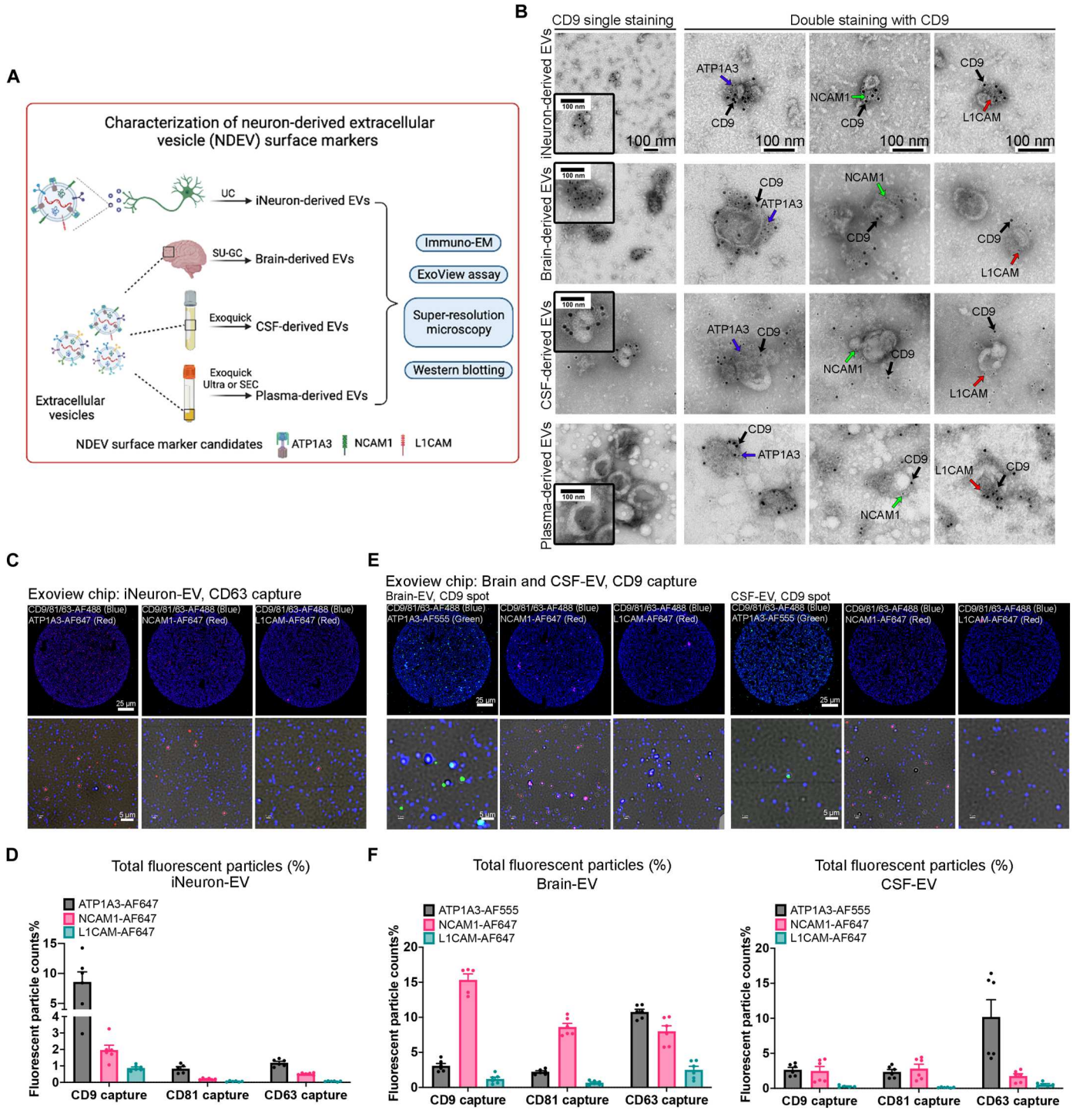

Fig. 1. ATP1A3 is a neuron-specific EV marker candidate besides NCAM1 and L1CAM and associated with EVs in human brain tissues and biofluids at a single-particle level. (**A**) Experimental design for evaluating whether NDEV marker candidates (ATP1A3, NCAM1, and L1CAM) is associated with EVs. UC, ultracentrifugation; SU-GC, sucrose gradient centrifugation; SEC, size exclusion chromatography. (**B**) Transmission electron micrograph showing immunogold labeling of EVs isolated from iNeuron, brain, CSF, and plasma stained with anti-CD9 antibody (10 nm) and anti-ATP1A3, NCAM1, and L1CAM antibody (5 nm). Scale bars, 100 nm. (**C**) Representative fluorescent images of iNeuron-EV detected by fluorescent-conjugated antibodies (red: ATP1A3-AF647, NCAM1-AF647 or L1CAM-AF647; blue: CD9/81C/63-AF488) on Exoview chip CD63 capture spots. The round circle in magnified images masks costained particles with tetraspanins. Scale bars, 25 and 5 μm. (**D**) Percentages of ATP1A3, NCAM1, and L1CAM fluorescent particle counts relative to total particles in iNeuron derived EVs (n = 2 biological replicates) on Exoview chip tetraspanins capture spots. (**E**) Representative fluorescent images of brain- and CSF-EV detected by fluorescent-conjugated antibodies (green: ATP1A3-AF555; red: NCAM1-AF647 or L1CAM-AF647; blue: CD9/81/63-AF488) on Exoview chip CD9 capture spots. The round circle in magnified images masks co-stained particles with tetraspanins. Scale bars, 25 and 5 μm. (**F**) Percentages of ATP1A3, NCAM1, and L1CAM fluorescent particle counts relative to total particles in brain (n = 2) and CSF (n = 2) derived EVs on Exoview chip tetraspanins capture spots.

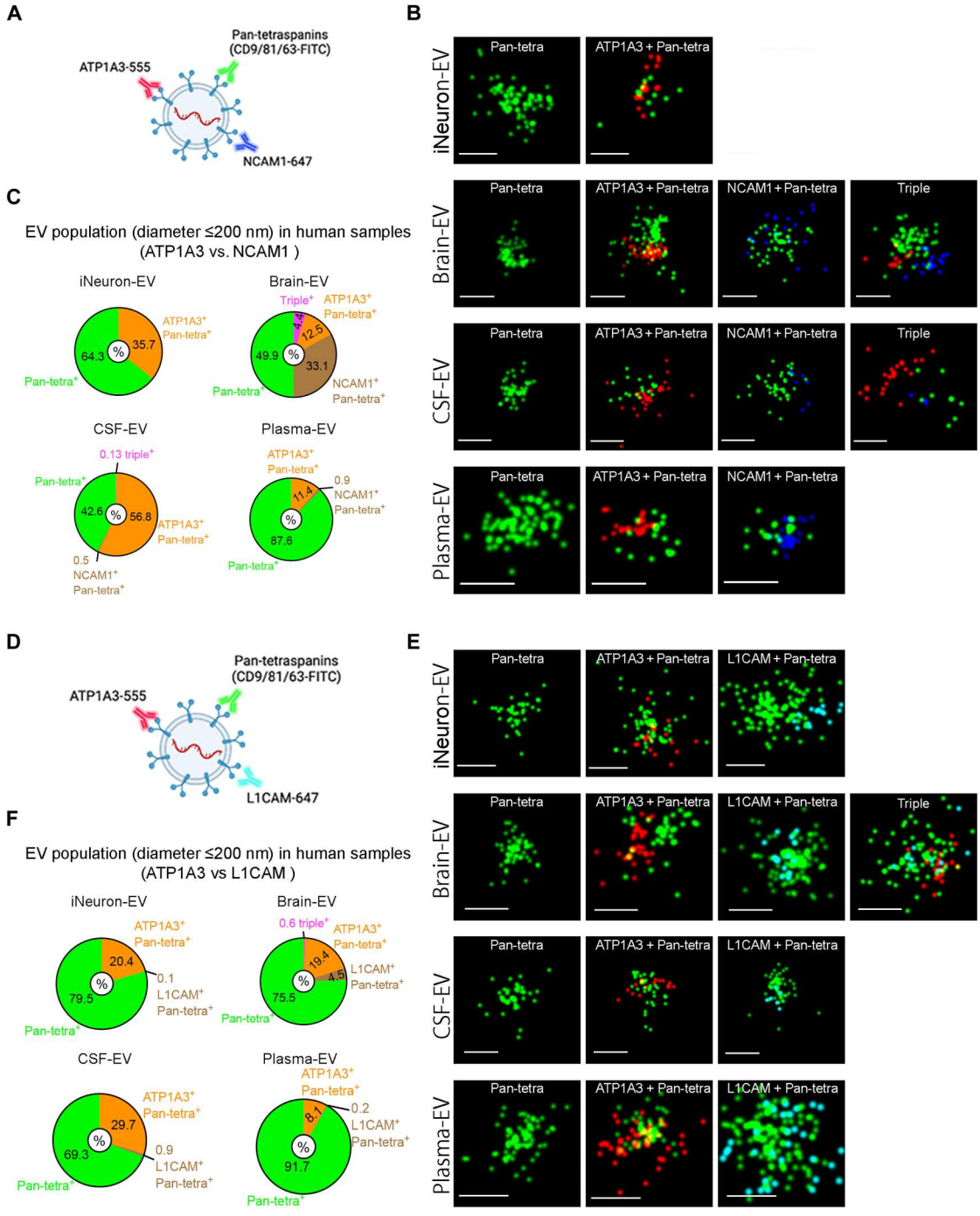

Fig. 2. Comparative analysis of NDEV candidate markers (ATP1A3, NCAM1, and L1CAM) expression in EVs by super-resolution microscopy. (**A**) Schematics showing the staining protocol of ATP1A3 and NCAM1 for EVs. (**B**) Representative super-resolution microscopy images showing the expression of ATP1A3 and NCAM1 in pan-tetraspanins (CD9/81/63) positive EVs at a single-particle level. Scale bars, 100 nm. (**C**) Pie charts showing the heterogeneous EV population with ATP1A3 and NCAM1 in different EV preparations. Particles with diameter less than 200 nm were quantified. (**D**) Schematics showing the staining protocol of ATP1A3 and L1CAM for EVs. (**E**) Representative super-resolution microscopy images showing the expression of ATP1A3 and L1CAM in pan-tetraspanins (CD9/81/63) positive EVs at a single-particle level. Scale bars, 100 nm. (**F**) Pie charts showing the heterogeneous EV population with ATP1A3 and L1CAM in different EV preparations. Particles with diameter less than 200 nm were quantified.

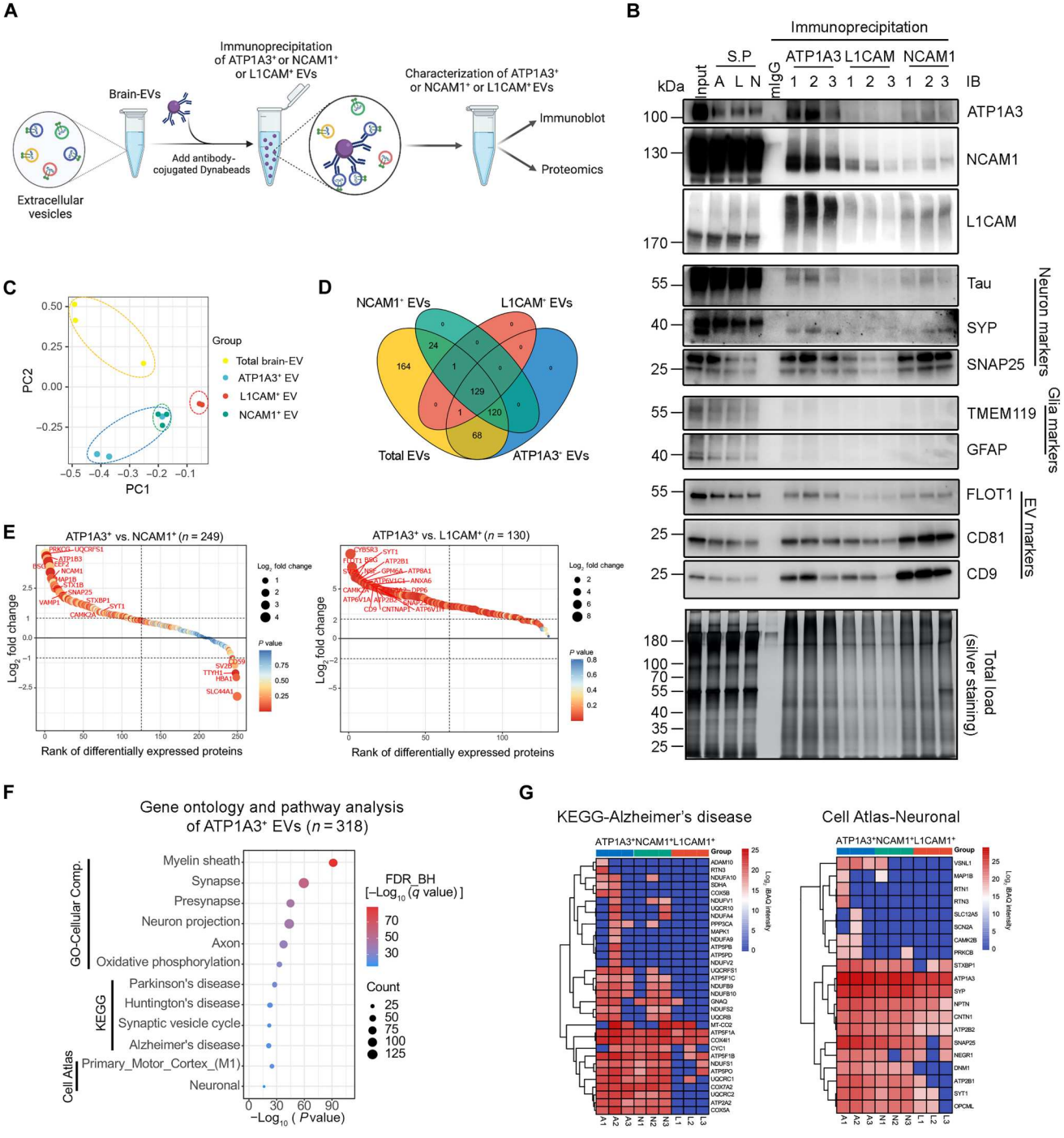

Fig. 3. ATP1A3$^+$ EV immunoprecipitated from human brain tissues displays higher neuronal cell type specificity. (**A**) Workflow for characterizing ATP1A3$^+$, NCAM1$^+$, and L1CAM$^+$ EVs immunoprecipitated from brain. (**B**) Western blot images of 5% total EVs (Input), supernatant (S.P), and immunoprecipitated EVs (A, ATP1A3; L, L1CAM; N, NCAM1) isolated from control brains (n = 3) and probed for neuron and glia markers. Equivalent proteins from brain-EVs were used for immunocapturing ATP1A3, L1CAM, and NCAM1. IB, immunoblotting antibody (**C**) Principal components analysis (PCA). The EV proteome of total brain-EV and immunoprecipitated EVs were measured in triplicate and classified. (**D**) Venn diagram showing the number of proteins differentially identified in total, ATP1A3$^+$, L1CAM$^+$, and NCAM1$^+$ brain-EVs by proteomics (n = 3 per group). (**E**) Gene ranking dotplot showing the DEPs in ATP1A3$^+$ brain-EVs compared to NCAM1$^+$ and L1CAM$^+$ brain-EVs. (**F**) Gene ontology, pathway, and cell type enrichment analysis of total identified proteins in ATP1A3$^+$ brain-EVs. (**G**) Heatmaps showing the expression level of proteins associated with Kyoto Encyclopedia of Genes and Genomes (KEGG) pathway term AD and Cell Atlas term Neuronal cell type within each immunoprecipitated EV sample.

enrichment of neuron-specific proteins, including microtubule-associated protein 1B, syntaxin-1B, SNAP25, synaptotagmin-1 (SYT1), and calcium/calmodulin-dependent protein kinase II alpha (CAMK2A) in ATP1A3$^+$ EVs versus NCAM1$^+$ EVs (Fig. 3E). Similarly, compared to L1CAM1$^+$ EVs, the top DEPs in ATP1A3$^+$ EVs also included neuronal proteins such as SYT1, CAMK2A, contactin-associated protein 1, and SNAP25 (Fig. 3E), demonstrating the superior enrichment of neuronal molecules in ATP1A3$^+$ EVs over NCAM1$^+$ or L1CAM1$^+$ EVs. Gene set enrichment analysis of affinity purified EVs demonstrated that proteins in ATP1A3$^+$, NCAM1$^+$, and L1CAM$^+$ EVs were significantly associated with not only synaptic molecules but also myelin sheath, neurodegenerative diseases, and oxidative phosphorylation (Fig. 3F and fig. S8B). Gene set enrichment analysis of 68 unique proteins in ATP1A3$^+$ EVs was also related to similar pathways, whereas 24 unique proteins in NCAM1$^+$ EVs were enriched in fatty acid biosynthesis, vesicle endocytosis, and secretion (fig. S8C). We examined proteins associated with AD and neuronal markers among three groups by heatmaps, showing unique enrichment of AD related molecules in ATP1A3$^+$ EVs: disintegrin and metalloproteinase domain-containing protein 10, reticulon-3, mitogen-activated protein kinase 1, and neuronal proteins: reticulon-1, sodium channel protein type 2 subunit alpha, and CAMK2B (Fig. 3G). These results revealed that cargo molecules in ATP1A3$^+$ EVs comprehensively reflect the neuronal and disease changes in the brain.

Increased Aβ level in ATP1A3$^+$ EVs derived from CSF and plasma of AD cases

We next sought to isolate potential NDEVs from human biofluids by immunocapturing ATP1A3 and other molecules to investigate its application to biomarker discovery for neurological diseases including AD (Fig. 4A). We extracted total EVs from CSF and plasma and immunocaptured NDEVs by specific antibodies. The immunocaptured target molecules were evaluated by Western blotting and enzyme-linked immunosorbent assay (ELISA) kits, showing the higher enrichment of ATP1A3 in EV fractions compared to immunocapture with NCAM1, L1CAM, or control isotype IgG antibody in CSF-EVs (fig. S9, A and B). We observed similar enrichment of ATP1A3 in plasma EVs but not NCAM1 or L1CAM using specific antibodies (fig. S10, A and B). In addition, the particle distribution of affinity-enriched ATP1A3$^+$, NCAM1$^+$, and L1CAM$^+$ CSF-EVs was evaluated by nanoparticle tracking analysis (fig. S11, A and B). The particle numbers were reduced after the immunoprecipitations of NDEVs, reflecting the selection by affinity enrichment (fig. S11B).

ATP1A3$^+$ CSF-EV samples were tested for quantification of AD biomarkers, including amyloid-β peptide 1-40 (Aβ40) and 1-42 (Aβ42), total tau (T-tau), p-tau at T181 (P-tau181) (*14*), and the neuronal protein SNAP25 using high-sensitivity digital ELISA (Simoa) (*15*). All of the AD biomarkers were detected in ATP1A3$^+$ CSF-EVs from both control and AD samples, although there was no difference due to the small sample size (Fig. 4B, n = 3 per group); SNAP25 was undetectable in AD samples, likely representing the synaptic loss in the AD brain (table S2 and Fig. 4B) (*16*). The Aβ42/40 ratio in ATP1A3$^+$ CSF-EVs was elevated in AD group compared to CSF or total CSF-EVs (Fig. 4C), suggesting the higher sensitivity for the detection of changes in Aβ42/40 ratio using ATP1A3$^+$ CSF-EVs compared to CSF or total CSF-EV samples.

Last, to investigate the diagnostic potential of plasma-derived ATP1A3$^+$ NDEVs as biomarkers in neurodegenerative diseases, we isolated plasma-EVs derived from age- and sex-matched 10 healthy controls (CTL), 10 mild cognitive impairment (MCI), and 10 patients with AD and performed single-particle analysis of EVs fluorescently stained with pan-tetraspanins (CD9/CD81/CD63), ATP1A3, and Aβ (clone 4G8) by dSTORM (Fig. 4D and fig. S12A). Particle size distribution of plasma-derived EVs was shown differently among the three groups (fig. S12, A and B). We observed the increased frequency of 50- to 100-nm particles in the MCI group compared to control and AD group, likely indicating an active release of small EVs in response of early pathological changes (*17*). The single EV-based quantitative analysis demonstrated a significantly higher percentage of Aβ$^+$ EV population in AD compared to healthy control and MCI (fig. S12C). Intriguingly, we observed a significant increase of Aβ$^+$ population in specified ATP1A3$^+$ EVs (Pan$^+$Aβ$^+$ATP1A3$^+$/Pan$^+$ATP1A3$^+$ ratio) in AD compared to control or MCI group (Fig. 4, E and F). To examine whether the elevation of Aβ$^+$ EV population in AD was specific to ATP1A3 associated EVs, we performed single-EV analysis of Aβ levels in NCAM1$^+$ and L1CAM$^+$ EVs from plasma samples of five controls and five patients with AD (fig. S13, A and C). In line with our findings depicted in Fig. 2, the number of NCAM1$^+$ and L1CAM$^+$ EVs in plasma was much fewer (fig. S13B, Pan$^+$NCAM1$^+$Aβ$^-$: CTL versus AD = 0.075% versus 0.408%, Pan$^+$NCAM1$^+$Aβ$^+$: CTL versus AD = 2.63% versus 1.33%; fig. S13D, Pan$^+$L1CAM$^+$Aβ$^-$: CTL versus AD = 1.178% versus 0.042%, Pan$^+$L1CAM$^+$Aβ$^+$: CTL versus AD: 3.78% versus 0.29%) than ATP1A3$^+$ EVs (fig. S12C, Pan$^+$ATP1A3$^+$Aβ$^-$: CTL versus AD = 50.85% versus 38.25%, Pan$^+$ATP1A3$^+$Aβ$^+$: CTL versus AD = 1.27% versus 14.13%). The very limited frequency of detecting NCAM1$^+$ and L1CAM$^+$ EVs in plasma has posed challenges in their utilization comparing to ATP1A3$^+$ plasma-EVs for biomarker development.

Furthermore, we found that Aβ$^+$ population in ATP1A3$^+$ plasma EV were positively correlated with tau pathology as defined by Braak stage and negatively correlated with cognitive assessments including Mini-Mental State Examination (MMSE) (*18*) and Dementia Rating Scale (DRS) (Fig. 4G) (*19*). We also quantified conventional AD blood biomarkers, including Aβ40, Aβ42, Aβ42/40 ratio, and total tau (T-tau) using the same total plasma samples by Simoa (table S3) (*20*). In total plasma, there is marginal but significant decrease of Aβ42/Aβ40 ratio in AD group compared to controls, while there was no difference in other parameters (Fig. 4H and fig. S14). We further analyzed receiver-operating characteristics (ROC) curves to compare the diagnostic accuracy of these potential plasma biomarkers. Across all the comparisons, the highest area under the curve (AUC) values were seen with % Aβ$^+$ population in ATP1A3$^+$ EVs: AUC values were 0.95 for AD versus controls (Fig. 4I) and 0.94 for AD versus MCI (Fig. 4J). AUCs for plasma Aβ42, Aβ40, Aβ42/Aβ40 ratio, and T-tau were 0.71, 0.52, 0.86, and 0.56 for AD versus controls (Fig. 4I) and 0.54, 0.61, 0.60, and 0.55 for AD versus MCI (Fig. 4J). Therefore, our findings demonstrated the potential of developing ATP1A3$^+$ EVs as promising diagnostic blood biomarkers for neurodegenerative disorders including AD.

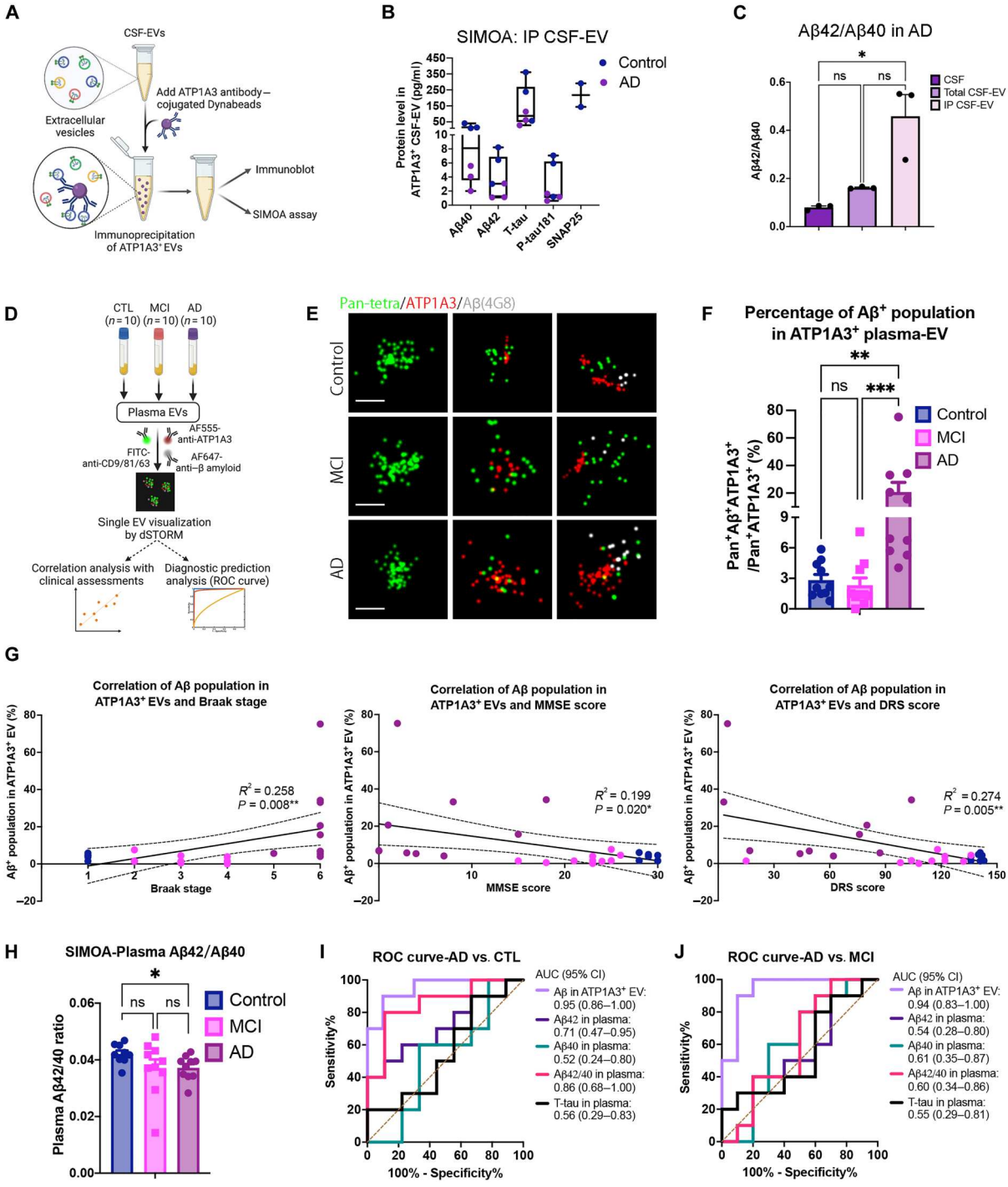

Fig. 4. ATP1A3$^+$ EV analysis in human CSF and plasma. (**A**) Workflow for characterizing ATP1A3$^+$ EVs immunoprecipitated from CSF. (**B**) Simoa quantification of AD related neuropathogenic proteins (Aβ42, Aβ40, T-tau, P-tau181, and SNAP25) in ATP1A3$^+$ CSF-EVs from healthy controls ($n = 3$) and AD ($n = 3$). Data are presented by box and whisker plot which shows the median and the 25th to 75th percentiles. (**C**) Aβ42/Aβ40 ratio in CSF, total CSF-EV, and ATP1A3 immunoprecipitation (IP) CSF-EV samples among AD group. (**D**) Workflow explaining single-particle analysis of Aβ$^+$ population in ATP1A3$^+$ plasma-EV to distinguish AD from healthy controls (CTL) and mild cognitive impairment (MCI). (**E**) Representative super-resolution microscopy images showing plasma-derived Aβ$^+$ ATP1A3$^+$ single EV among control, MCI, and AD groups [green: FITC-CD9/81/63, red: Alexa Flour 555-ATP1A3, gray: Alexa Flour 647-Aβ (clone 4G8)]. Scale bars, 100 nm. (**F**) Percentage of Aβ$^+$ population in ATP1A3$^+$ plasma-EV among control, MCI, and AD groups ($n = 10$ per group). (**G**) Correlations of Aβ$^+$ population in ATP1A3$^+$ plasma-EV with clinical Braak stage, Mini-Mental State Examination (MMSE), and Dementia Rating Scale (DRS) scores in combined control ($n = 7$), MCI ($n = 10$), and AD ($n = 10$) samples. The dashed line indicates 95% confidence band of the best-fit line. Pearson correlation coefficients are shown. (**H**) Quantification of Aβ42/Aβ40 level in total plasma samples from CTL ($n = 9$), MCI ($n = 10$), and AD ($n = 10$). (**I** to **J**) Receiver-operating characteristics (ROC) curves displaying the performance of Aβ$^+$ population in ATP1A3$^+$ plasma-EV, plasma Aβ40, Aβ42, Aβ42/Aβ40 ratio, and T-tau to distinguish (I) AD from CTL and (J) AD from MCI. T-tau, total tau; AUC, area under the curve; CI, confidence interval; ns, no significance; *P < 0.05, **P < 0.01, ***P < 0.001.

DISCUSSION

By following the Minimal Information for Studies of Extracellular Vesicles (MISEV) 2018 guidelines (*21*), we used multiple methods to validate that ATP1A3 is associated with EVs as a promising NDEV marker in human brain, CSF, and plasma. Unlike the most frequently used marker L1CAM and NCAM1 (*2*), ATP1A3 expression is more restricted to neurons in the CNS and enriched in EVs from brain and biofluids. Although the potential degradation and alterations in the integrity of EVs from frozen postmortem brain tissues may affect the quality of the isolated EVs (*22*), our work successfully characterized the EV-specific protein cargos immunoprecipitated from human brain samples and demonstrated that ATP1A3$^+$ EVs exhibited higher enrichment of neuronal molecules than L1CAM1$^+$ and NCAM1$^+$ EVs. These findings indicate that ATP1A3 represents a bona fide NDEV marker. We further showed a clear presence of ATP1A3$^+$ EV in human CSF and plasma samples, revealing the high potential to access NDEVs from a liquid biopsy. Notably, Aβ$^+$ population in ATP1A3$^+$ plasma-EV displayed a better discrimination of AD from healthy controls and MCI than conventional biomarkers, showing the optimism to explore promising blood biomarkers for neurodegenerative diseases by isolating circulating NDEVs. A potential limitation of our study is the presence of clinical heterogeneity, which may arise from the small sample size of 10 subjects per group. Therefore, future studies investigating AD or other disease-associated molecules including tau, TDP-43, and α-synuclein in ATP1A3$^+$ EVs from plasma with larger cohorts and multicentered samples would provide significant insights for disease diagnosis. Application of dSTORM as a single-EV analysis platform will enable us to characterize the loading of disease-specific biomarkers at single-molecule resolution, which may potentially improve the sensitivity and accuracy of disease detection (*23*). Our results propose ATP1A3 as a reliable target to enrich NDEVs from human samples and pave a fresh way to study molecular changes associated with neurological diseases in the CNS.

MATERIALS AND METHODS

Brain, CSF, and plasma sample acquisitions

One cohort of brain tissues from healthy controls, two cohorts of CSF, and two cohorts of plasma samples including healthy control and AD cases were used in this study. The postmortem brain tissues (superior temporal lobe) were obtained from Boston University School of Medicine Brain Bank. The first cohort of control CSF used for immuno-gold staining, ExoView analysis, super-resolution imaging, Western blotting, and ELISA was obtained from the Greater Los Angeles Veteran's Affairs Hospital as a part of National Institutes of Health (NIH) NeuroBioBank. The second cohort of CSF used for Simoa analysis was acquired from Banner Sun Health Research Institute (three AD and three healthy controls). The first cohort of control plasma samples used for immuno-gold staining, super-resolution imaging, Western blotting, and ELISA was obtained from Boston University School of Medicine. The second cohort of plasma used for β amyloid analysis by super-resolution microscopy and Simoa was acquired from the University of California, San Diego (10 healthy controls, 10 MCI, and 10 AD). All the AD, MCI, and control cases were neuropathologically diagnosed by Braak stages for tau and Thal stages for β amyloid and with short postmortem intervals. We performed clinical testing by the MMSE to classify individuals with MCI and AD. Participants with an MMSE score between 23 and 27 were categorized as MCI, while those with an MMSE score below 23 were categorized as AD. Human subjects from these three groups were carefully matched for age [CTL versus MCI versus AD = 82.7 versus 88.5 versus 82.5 years old, analysis of variance (ANOVA) $P > 0.05$] and sex (five male and five female for each group). The demographic information of all cases is provided in table S4. The Institutional Review Board at Boston University Medical Campus, the University of California, San Diego, the Greater Los Angeles Veteran's Affairs Hospital, and the Banner Health Institute approved the brain the protocol, and all participants provided informed consent. This work was approved by the Mayo Clinic Institutional Review Board. Biosafety protocols were in compliance with the Institutional Biosafety Committee of Mayo Clinic.

EV isolation from induced hiPSC neurons (iNeurons)

Rapid induction of induced pluripotent stem cell (iPSC) into human excitatory neurons was performed via a doxycycline-inducibleNGN2 system using our published protocol (*24*). Briefly, to initiate NGN2 induction, doxycycline was added to NGN2 iPSCs at a final concentration of 2 μg/ml in fresh media consisting of KnockOut Dulbecco's modified Eagle's medium (catalog no. 10829018), KnockOut Serum Replacement (catalog no. 10828010), MEM Non-Essential Amino Acids (NEAA) solution (catalog no. 11-140-050), GlutaMAX (catalog no. 35050061), and β-mercaptoethanol (catalog no. 21985023, all from Invitrogen). On Day 2, puromycin was added at 5 μg/ml for selection. On D4, cells were replated on poly-ornithine (10 μg/ml; catalog no. P4957, Sigma-Aldrich) and mouse laminin (5 μg/ml; catalog no. 23017015, Invitrogen) co-coated six-well plate (1×10^6 cells per well) in media consisting of Neurobasal (catalog no. 21103049, Gibco), B27 (catalog no. 17504044, Gibco), GlutaMAX, 20% dextrose (catalog no. G8769, Sigma-Aldrich), MEM-NEAA supplemented with brain-derived neurotrophic factor (10 ng/ml; catalog no. 450-02), glial cell line–derived neurotrophic factor (catalog no. 450-10), and ciliary neurotrophic factor (catalog no. 450-13, all from PeproTech). Conditioned media from D17 to D21 was collected and processed for iNeuron-EV isolation by ultracentrifugation at 110,000*g* overnight at 4°C in a 41Ti rotor (Optima-XE SW41, Beckman Coulter). EVs were resuspended in phosphate-buffered saline (PBS) for further characterization.

EV isolation from human brain, CSF, and plasma

The unfixed frozen tissue (0.5 g) from temporal cortex of deceased control cases was processed for EV extraction based on reported method with some modifications (*4*, *25*). Briefly, the tissue was sliced with a razor blade into 2- to 3-mm^3 sections on ice. The cut sections were dissociated in Hibernate-E medium (catalog no. A1247601, Thermo Fisher Scientific) containing collagenase type 3 (75 U/ml; catalog no. LS004180, Worthington Biochemical) at 37°C for 15 min. After incubation, the tissue samples were immediately added with protease inhibitor (catalog no. PI78443, Thermo Fisher Scientific) and 6 ml of ice-cold Hibernate-E without further homogenesis and filtered with 40-μm mesh filter (catalog no. 22-363-547, Thermo Fisher Scientific). After filtration, the samples were sequentially centrifuged at 300*g* for 10 min at 4°C to precipitate large debris, 2000*g* for 10 min at 4°C to precipitate cellular fraction,

and 5000*g* for 20 min at 4°C to precipitate plasma membrane fraction. The supernatant was filtered using a 0.45-μm polyethersulfone membrane filter (catalog no. SLHPM33RS, Millipore) and ultracentrifuged at 110,000*g* for 70 min at 4°C using a SW41Ti rotor. The pellet was resuspended in 2 ml of 0.475 M sucrose solution (catalog no. S5-3, Thermo Fisher Scientific). The sucrose step gradient was further created with steps starting from 2.0 to 1.5, 1.0, 0.825, 0.65, and 0.475 M to facilitate capture of the EV-rich pellet by centrifuging at 200,000*g* for 20 hours at 4°C. The final pellet from "V" (the fraction between 0.65 and 0.825 M) and "VI" (the fraction between 0.825 and 1.0 M) was combined as brain-derived EV pellet.

For CSF-derived EV extraction, we used the commercial ExoQuick EV isolation kit (catalog no. EXOQ5A-1, System Biosciences) according to the manufacturer's instructions. For all the experiments, pooled CSF were used. Briefly, 1-ml CSF sample was thawed on ice and added with protease inhibitor and centrifuged at 3000*g* for 20 min at 4°C. The supernatant was transferred to a new tube and centrifuged at 5000*g* for 20 min at 4°C. The supernatant from CSF was then added with the appropriate volume of ExoQuick precipitation solution and incubated overnight at 4°C. The mixture was centrifuged at 1500*g* for 30 min at 4°C to precipitate the EV pellet, respectively. For plasma sampling, 500 μl was thawed on ice and added with protease inhibitor and centrifuged at 1500*g* for 10 min at 4°C, and then the supernatant was centrifuged at 10,000*g* for 20 min at 4°C. Subsequently, an ExoQuick ULTRA EV isolation kit (catalog no. E Q ULTRA-20A-1, SBI) was used to isolate plasma-EV designated for immunoblotting according to the manufacturer's instructions. Otherwise, we used qEV original columns (IZON Science, MA, USA) to separate enriched EV fractions from plasma as previously described (*26*).

Immunofluorescent staining

For human brain sections, sequential deparaffinization and antigen retrieval in 1 × Co-Detection Target Retrieval Reagent (Advanced Cell Diagnostics, USA) for 15 min at 98°C was performed; for mouse brain sections, antigen retrieval was performed in sodium citrate for 20 min at 95°C and rinsed two times with PBS; for the cultured cells, they were washed three times with 1 × Dulbecco's PBS and fixed in 4% paraformaldehyde at 37°C for 15 min, before embedding into blocking buffer [1× PBS, 5% bovine serum albumin (BSA; A7906, Sigma-Aldrich), 5% goat (catalog no. 16210-064, Thermo Fisher Scientific) or donkey serum (D9663, Sigma-Aldrich), and 1% Triton X-100 (T9284, Sigma-Aldrich)] at room temperature for 1 hour. The samples were then labeled overnight at 4°C, and the primary antibodies used were anti-ATP1A3 (1:1000, catalog no. MA3915, Thermo Fisher Scientific), anti-NCAM1 (1:1000, catalog no. MA5-11563, Thermo Fisher Scientific), anti-L1CAM (1:1000, catalog no. 14-1719-82, Thermo Fisher Scientific), anti-MAP2 (1: 200, catalog no. 13-1500, Thermo Fisher Scientific), anti-GFAP (1:2500, Z033429, Agilent), and anti-IBA1 (1:100, 019-19741, Wako Chemicals). Alexa Fluor secondary antibodies (Life Technologies) were conjugated to the target species at room temperature (25°C) for 1 hour. DAPI (4′,6-diamidino-2-phenylindole; 1:2500, Thermo Fisher Scientific, D1306) was used to label the nuclei. Images were acquired using a Leica SP8 confocal microscope (Leica). All animal procedures followed the guidelines of the NIH Guide for the Care and Use of Laboratory Animals and were approved by the Mayo Clinic Institutional Animal Care and Use Committee.

Immunogold labeling of EVs on transmission electron microscopy

The immunogold labeling of EVs (purified iNeuron-EV, brain-EV, CSF-EV, and plasma-EV) was analyzed at the Electron Microscopy Facility, Harvard Medical School, as previously described (*11*). For single immunogold labeling of CD9 on isolated EVs, 5 μl of the samples containing 1×10^{10} particles/ml was adsorbed for 5 min to carbon-coated grids (CF400-CU, Electron Microscopy Sciences) that had been made hydrophilic by a 20-s exposure to a glow discharge (25 mA). After adsorption, the grids were blocked on 1% BSA (catalog no. A7906, Sigma-Aldrich) for 10 min, transferred to 5-μl drops of primary mouse anti-human CD9 antibody (1:20, catalog no. 555370, BD Biosciences), and incubated for 30 min and then washed in four drops of PBS (total 10 min) before incubation in rabbit anti-mouse bridging antibody (1:50, catalog no. ab6709, Abcam) for 30 min followed by PBS washes and incubation in 5-nm protein A-gold (University Medical Center, Utrecht, The Netherlands) for 20 min. Grids were washed in two drops of PBS followed by four drops of water (total 15 min) and subsequent staining in 1% uranyl acetate. After removing the excess uranyl acetate with a filter paper, the grids were examined in a JEOL 1200EX transmission electron microscope, and images were recorded with an AMT 2k charge-coupled device camera.

For double immunogold labeling of EVs, the grids were fixed for 1 min in 1% glutaraldehyde, quenched on four drops of 20 mM glycine in PBS for a total of 10 min following the first primary antibody (anti-ATP1A3, catalog no. MA3915; anti-NCAM1, catalog no. MA5-11563; anti-L1CAM, catalog no. 14-1719-82; all from Thermo Fisher Scientific) and 5-nm protein-A incubation and PBS washes. The labeling procedure was repeated with a second primary antibody (CD9, 1:30), followed by rabbit anti-mouse and a larger size protein A gold (10 nm). The grids were stained in uranyl acetate and imaged as described above.

Super-resolution microscopy

Super-resolution images of EVs were acquired using dSTORM from ONI (Nanoimager S, Oxford Nanoimaging, UK) equipped with a 100×, 1.4 numerical aperture oil immersion objective. EV samples were immobilized on microfluidic glass slides (EV profiler Kit, EV-MAN-1.0, Oxford Nanoimaging) and stained with pan-tetraspanin antibodies cocktail consisting of fluorescein isothiocyanate (FITC) anti-human CD9 (HI9a, catalog no. 312104), FITC anti-human CD81 (5A6, catalog no. 349504), and FITC anti-human CD63 (H5C6, catalog no. 353006; all from BioLegend), anti-ATP1A3 antibody (catalog no. MA3915, Thermo Fisher Scientific) conjugated to Alexa Flour 555 fluorophore by commercial conjugation kit (ab269820, Abcam), AF647-conjugated anti-NCAM1 antibody (catalog no. 563443, BD Biosciences), or AF647-conjugated anti-L1CAM antibody (catalog no. 564194, BD Biosciences) according to the manufacturer's instructions as described (*10*). Two thousand five hundred total images were recorded for localization mapping using 30, 30, and 30% power on the 488-, 561-, and 640-nm lasers, respectively. Colocalization analysis of the different molecules in a single EV was proceeded with the CODI online analysis platform (https://alto.codi.bio/). Localization clusters with more than 15 individual molecules were regarded as EVs. EV clusters with *Skew* ranging from 1 to 2.9 and *Circ* ranging from 0.43 to 1 were selected for further analysis. A marker was considered as positive in a single particle when more than three individual molecules

were detected in the same channel within a radius of 100 nm around the center of a cluster. Five fields of view were acquired from each sample for quantitative analysis. Furthermore, to visualize and analyze the neurodegenerative disease–associated proteins by dSTORM, plasma-derived EVs were stained with FITC anti-tetraspanins (CD9, CD63, and CD81), AF555-conjugated anti-ATP1A3 and AF647-conjugated anti–β amyloid (catalog no. 800718, BioLegend), AF647-conjugated anti-NCAM1, or AF647-conjugated anti-L1CAM and AF594-conjugated anti–β amyloid antibodies (catalog no. 800716, BioLegend). Three thousand total images were recorded for localization mapping using 30, 30, and 30% power on the 488-, 561-, and 640-nm lasers, respectively. Aβ was considered as positive in a single particle when more than two individual molecules were detected in the same channel within a radius of 200 nm around the center of a cluster. Six fields of view were acquired from each sample for quantitative analysis by CODI platform.

SP-IRIS analysis

SP-IRIS analysis of iNeuron-EV, brain-EV, and CSF-EV was performed on ExoView Tetraspanin chips (EV-TC-TTS-01, NanoView Biosciences) using the ExoView R100 platform (NanoView Biosciences, Boston, USA) as described (*9*, *10*). Desired volume of EVs was diluted in buffer A to a final volume of 40 μl. Thirty-five microliters of each diluted sample was incubated on ExoView Tetraspanin Chip for 16 hours at room temperature. The chips contained spots printed with anti-EV markers including CD63, CD81, and CD9 for EV capturing, or mouse IgG antibody, used as a control for nonspecific EV binding. The chips were then washed three times in 1-ml solution A and followed by incubation for 1 hour at room temperature with labeling antibodies. In our experiment, EV antibodies cocktail (EV-TC-AB-01, NanoView Biosciences) containing AF488-conjugated anti-CD63, anti-CD81, and anti-CD9 antibodies, AF647-conjugated anti-ATP1A3 antibody (NBP2-99238AF647, Novus Biologicals), AF647-conjugated anti-NCAM1 antibody (catalog no. 563443, BD Biosciences), and AF647-conjugated anti-L1CAM antibody (catalog no. 564194, BD Biosciences) were used for detection of EV subpopulations. In addition, the Alexa Fluor 555 Conjugation Kit (ab269820, Abcam) was used to conjugate AF555 fluorophores with anti-ATP1A3 antibody (catalog no. MA3915, Thermo Fisher Scientific) according to the manufacturer′s protocol. All the antibodies were prediluted 1:500 in solution A. After 1-hour incubation at room temperature, the chips were washed, dried, and then imaged with the ExoView R100 reader using the ExoView Scaner 3.0 acquisition software. The data were then analyzed using ExoView Analyzer 3.0. The signal recorded on mouse IgG-printed spots was used as background control for normalization. The percentage of $ATP1A3^+$ EVs, $NCAM1^+$ EVs, or $L1CAM^+$ EVs in each anti-tetraspanin spot was calculated as the ratio of AF555-positive events or AF647-positive events to the total fluorescent events × 100. The heatmaps showing total fluorescent particle counts were generated using Graphpad Prism 9. Two biological replicates for iNeuron-EV, brain-EV, and CSF-EV were used for the assessment.

Western blotting

Brain tissues, CSF, plasma, and corresponding EV fractions were lysed in cold radioimmunoprecipitation assay (RIPA) buffer [25 mM tris-HCl (pH 7.6), 150 mM NaCl, 1% NP-40, 1% sodium deoxycholate, and 0.1% SDS; catalog no. 89900, Thermo Fisher Scientific] supplemented with a protease and phosphatase inhibitor mixture (catalog no. 78445, Thermo Fisher Scientific) and sonicated for 5 min. Protein concentration was measured by microBCA assay (catalog no. 23235, Thermo Fisher Scientific). The equivalent amounts of brain lysates, CSF, plasma, or EVs were denatured in Laemmli sample buffer (catalog no. 1610737, Bio-Rad) and loaded on 4 to 20% Tris-Glycine eXtended (TGX) stain-free SDS–polyacrylamide gel electrophoresis (SDS-PAGE) gels (catalog no. 4568096, Bio-Rad) or normal SDS-PAGE gels (catalog no. 4561096, Bio-Rad) and then electro-transferred to 0.45-μm nitrocellulose membranes (catalog no. 1620115, Bio-Rad). The membranes were blocked with 5% nonfat milk (catalog no. 9999S, Cell Signaling Technology) and incubated with primary antibodies overnight at 4°C. The following primary antibodies were used for immunoblots: anti-NCAM1 (1:500, Thermo Fisher Scientific, MA5-11563), anti-ATP1A3 (1:500, Thermo Fisher Scientific, MA3915), anti-L1CAM (1:200, Thermo Fisher Scientific, 14-1719-82), anti-CD81 (1:500, BioLegend, 349502), anti-CD9 (1:500, Millipore, CBL162), anti-CytoC (1:200, Cell Signaling Technology, 11940S), anti-GM130 (1:100, Santa Cruz Biotechnology, sc55591), anti-H2A (H2A.Z, 1:200, Cell Signaling Technology, 2718S), anti-Tau (Tau13, 1:1000, distributed by Kanaan lab), anti-GAPDH (1:500, Thermo Fisher Scientific, MA5-15738), anti-SYP (1:500, Sigma-Aldrich, S5768), anti-SNP25 (1:500, BioLegend, 836304), anti-TMEM119 (1:500, Sigma-Aldrich, HPA051870), anti-GFAP (1:500, Dako, z0334), anti-FLOT1 (1:1000, BD Biosciences, 610820), anti-annexin A2 (1:500, Abcam, ab178677), anti-APOA1 (1:100, Santa Cruz Biotechnology, sc-376818), and anti–β-actin (1:500, Santa Cruz Biotechnology, sc-47778). The membrane was further incubated with appropriate horseradish peroxidase (HRP)–labeled secondary antibodies (anti-mouse IgG, HRP-linked antibody, Cell Signaling Technology, 7076S; anti-rabbit IgG, HRP-linked antibody, Cell Signaling Technology, 7074S) for 1 hour, and immunoreactivity was captured using enhanced chemiluminescence solutions (catalog no. WBKLS0100, Millipore). For silver staining, the protein gels were fixed and stained according to the manufacturer′s instructions (catalog no. 24612, Thermo Fisher Scientific). All the images were detected using the ChemiDoc MP Imaging System (Bio-Rad). For the quantification analysis, the band densities were digitally measured by ImageJ software (NIH).

For proteinase protection assay shown in fig. S7, the equivalent amounts of brain-derived EVs (5 μg) were incubated with proteinase K (PK; 20 μg/ml; catalog no. 19131, QIAGEN) and 5 mM $CaCl_2$ in PBS for 1 hour at 37°C with gentle vortexing every 15 min. The EVs with or without PK treatment were loaded for immunoblotting as described above.

Immunocapture of $ATP1A3^+$, $NCAM1^+$, and $L1CAM^+$ EVs from brain, CSF, and plasma

Immunocapture of specific EVs from bulk EVs was performed according to our previous publication with minor modifications (*4*). The antibodies against potential NDEV markers ATP1A3 (Thermo Fisher Scientific, MA3915), NCAM1 (Thermo Fisher Scientific, MA5-11563), and L1CAM (Thermo Fisher Scientific, 14-1719-82) were conjugated, respectively, to Dynabeads M-270 Epoxy using the Dynabeads Antibody Coupling Kit (catalog no. 14311D, Thermo Fisher Scientific) according to the manufacturer′s instructions. The equal amounts of total brain-EVs (40 μg) isolated from three

individual healthy controls or pooled CSF-EVs (25 μg) isolated from healthy controls or AD cases were initiated for immunoprecipitation. The EV samples were pretreated with 20 μl of human FcR receptor blocking solution (catalog no. 130-059-901, Miltenyi Biotec) on the ice for 15 min and then incubated with antibody-conjugated bead complex (5 μg/mg) in a final volume of 500 μl. As a negative control, IgG-conjugated beads were added to the mixed EVs from brain or CSF samples. After overnight incubation at 4°C, immunoprecipitated NDEVs were eluted in the equal volume of cold RIPA buffer containing protease inhibitor and divided for downstream mass spectrometry, Western blotting, and ELISA. The immunoprecipitated EVs were filtered in a 0.45-μm Spin-X centrifuge tube (catalog no. CLS8162, Corning) to completely remove magnetic beads. The total EVs and immunocaptured EVs were proceeded for immunoblotting as previously described. For EV particle analysis, IgG elution buffer (catalog no. 21028T, Thermo Fisher Scientific) was used for the elution, following by pH neutralization with 1 M tris buffer.

Mass spectrometry and data analysis

Total brain-EV (5 μg; $n = 3$) and immunoprecipitated EVs ($n = 3$ for NDEVs; $n = 2$ for mIgG control) were subjected to label-free quantitative mass spectrometry as previously described (*27*). First, EV samples were resuspended in 1× Laemmli sample buffer (catalog no. 1610747, Bio-Rad) with 2-mercaptoethanol and heated at 95°C for 5 min. The sample was loaded to 10% SDS-PAGE gel (catalog no. 4561033, Bio-Rad) and run until 1 cm off the loading well. The entire protein region of the gel was excised after Coomassie staining and subjected to in-gel trypsin digestion after reduction with dithiothreitol and alkylation with iodoacetamide. Peptides eluted from the gel were lyophilized and reconstituted in 25 to 50 μl of 5% acetonitrile containing 0.1% (v/v) formic acid (Suprapur, catalog no. 1116700250, EMD Millipore Corporation) with 1 pmol of yeast alcohol dehydrogenase 1 (ADH) digest and analyzed on a NanoAcquity Ultra Performance LC (UPLC) system (Waters Corporation, Milford, MA) coupled to a Orbitrap Fusion Lumos Tribrid mass spectrometer (Thermo Fisher Scientific Inc., Waltham, MA). A 1- to 2-μl injection was loaded at 4 μl/min for 4 min onto a custom-packed fused silica pre-column [kasil frit, 100 μm internal diameter (I.D.)] with 2 cm of ProntoSIL C18AQ (Bischoff Chromatography, 200 Å, 5 μm). Peptides were then separated on a 75 μm I.D. fused silica analytical column packed with 25-cm Magic C18AQ (Bruker-Michrom, 100 Å, 3 μm) particles to a gravity-pulled tip. Peptides were eluted at 300 nl/min using a linear gradient from 5 to 35% of mobile phase B [0.1% (v/v) formic acid in acetonitrile] in mobile phase A [0.1% (v/v) formic acid in water] in 115 min. Ions were introduced by positive electrospray ionization via liquid junction at 1.4 to 1.6 kV into a Orbitrap Fusion Lumos Tribrid mass spectrometer. Mass spectra were acquired from mass/charge ratio (m/z) 300 to 1750 at a resolution of 120,000 (m/z 200), maximum injection time of 50 ms using an AGC target of 4×10^5, and data-dependent acquisition (3-s cycle time) for tandem mass spectrometry by HCD fragmentation using an isolation width of 1.6 Da, max fill time of 22 ms, with an AGC target of 5×10^4. Peptides were fragmented using a collision energy of 30%, and fragment spectra were acquired at a resolution of 15000 (m/z 200).

Then, raw data files were processed with Proteome Discoverer (Thermo Fisher Scientific, version 2.1) and searched with Mascot Server (Matrix Science, version 2.6) against the Human (Swiss-Prot) FASTA file (downloaded 9 April 2019). Tryptic specificity (up to two missed cleavages), a 10-ppm mass tolerance for the precursor, and a 0.05-Da mass tolerance for the fragments were used as search parameters. All nonfiltered search results were processed by Scaffold (Proteome Software Inc., version 5.1.0) with threshold values set at 95% for peptides and 99% for proteins (two peptide minimum) using the Trans-Proteomic Pipeline (Institute for Systems Biology). Immunoprecipitated proteins were further selected after exclusion of keratins as contaminates and nonspecific proteins coimmunoprecipitated by isotype control IgG.

The protein comparison was conducted using the label-free intensity-based absolute quantification (iBAQ) method and further normalized by the average of ADH iBAQ across all the samples. The 0 iBAQ values were replaced with 1 for calculation purposes. Fold expression of overlapping proteins in $ATP1A3^+$ EVs versus $NCAM1^+$ EVs and $ATP1A3^+$ EVs versus $L1CAM1^+$ EVs was calculated from the individual median averaged protein normalized iBAQ values within each group. Functional pathway analyses including Gene Ontology analysis, Kyoto Encyclopedia of Genes and Genomes pathway analysis and Cell Atlas enrichment analysis of potential NDEV signatures were performed using the ToppGene Suite online tool (*28*) with false discovery rate (FDR) corrected P value <0.05 (https://toppgene.cchmc.org/). The heatmaps showing AD-related proteins and neuronal type proteins among $ATP1A3^+$ EVs, $NCAM1^+$ EVs, and $L1CAM^+$ EVs were generated using log2 iBAQ protein intensity. The final visualization of Venn diagram, gene ranking doplots, pathway bubble plots, and heatmaps was performed using R program (version 4.1.0).

Enzyme-linked immunosorbent assay

Commercial ELISA kits were used to evaluate the protein concentration of ATP1A3 (catalog no. OKEH05672, Aviva Systems Biology), NCAM1 (catalog no. ab119587, Abcam), and L1CAM1 (catalog no.ab278114, Abcam) in immunocaptured EVs from CSF and plasma according to the manufacturer′s instructions. Duplicated wells were performed in each assay. We had four biological replicates for each group.

Nanoparticle tracking analysis of EVs

The size distribution and concentration of EVs were analyzed by nanoparticle tracking analysis using a NanoSight NS300 instrument (Malvern, Worcestershire, UK). Isolated EVs from iNeuron, brain or CSF was prediluted in filtered PBS to achieve a concentration within the 107 to 108 range for optimal analysis. For each sample, 700-μl diluted EVs were injected into the sample-carrier cell, and the particles were automatically tracked and sized using Brownian motion and diffusion coefficients to record four videos of 30 s. The parameters were set at 22.5° ± 0.5°C for detection level 5 and camera levels 13 to 15. The size mode (nanometers), mean size (nanometers), and concentration (particle number per milliliter) of the EVs were calculated by combining the data from the four records.

Simoa assays

Simoa assays including Neurology 3-Plex A (TAU, Aβ42, and Aβ40), P-tau181 (V2), and SNAP-25 were conducted on the Simoa HD-X analyzer according to the manufacture′s instruction (Quanterix). Pooled CSF, corresponding total CSF-EVs and $ATP1A3^+$ EVs (45 μl in elution buffer) from healthy controls ($n =$

3) or AD (n = 3), were lysed with equal amount of M-PER Mammalian Protein Extraction Reagent (catalog no. 78503, Thermo Fisher Scientific) and protease inhibitor cocktail (catalog no. 78442, Thermo Fisher Scientific). IgG immunoprecipitation from mixed CSF-EVs was used as a negative control. CSF samples were centrifuged at 10,000g for 5 min, and plasma were centrifuged at 2000g for 10 min at 4°C before dilution with assay specific sample diluent provided in assay kits. The relative concentration estimates were calculated according to the sample standard curve. Data collection was conducted using Microsoft Excel, while analysis and graphing were performed using GraphPad Prism (version 9.0).

Statistical analysis

All data are presented as mean ± SEM where indicated. Statistical analyses including the calculation of Pearson correlation coefficients for correlation analysis and AUC values from ROC analysis were performed using GraphPad Prism (version 9.0). Comparisons within two groups were analyzed for significance using Student's unpaired two-tailed t test or paired two-tailed t test; Comparisons among three or more groups were performed with ordinary one-way ANOVA with Tukey's post hoc test or Kruskal-Wallis nonparametric ANOVA with Dunn's post hoc test if the data failed to pass normality tests of Shapiro-Wilk. Statistical significance was defined as P value < 0.05. P values in functional enrichment analyses were adjusted for multiple comparisons using FDR correction with the Benjamini-Hochberg method where indicated. Boxplots represent the median, 25th, and 75th percentiles, and whiskers represent measurements to the 5th and 95th percentiles.

Supplementary Materials

This PDF file includes:
Figs. S1 to S14
Legend for tables S1 to S4
Legend for source data

Other Supplementary Material for this manuscript includes the following:
Tables S1 to S4
Source data

REFERENCES AND NOTES

1. Y. You, T. Ikezu, Emerging roles of extracellular vesicles in neurodegenerative disorders. *Neurobiol. Dis.* **130**, 104512 (2019).
2. D. E. Gomes, K. W. Witwer, L1CAM-associated extracellular vesicles: A systematic review of nomenclature, sources, separation, and characterization. *J. Extracell. Biol.* **1**, (2022).
3. M. Norman, D. Ter-Ovanesyan, W. Trieu, R. Lazarovits, E. J. K. Kowal, J. H. Lee, A. S. Chen-Plotkin, A. Regev, G. M. Church, D. R. Walt, L1CAM is not associated with extracellular vesicles in human cerebrospinal fluid or plasma. *Nat. Methods* **18**, 631–634 (2021).
4. Y. You, S. Muraoka, M. P. Jedrychowski, J. Hu, A. K. McQuade, T. Young-Pearse, R. Aslebagh, S. A. Shaffer, S. P. Gygi, M. Blurton-Jones, W. W. Poon, T. Ikezu, Human neural cell type-specific extracellular vesicle proteome defines disease-related molecules associated with activated astrocytes in Alzheimer's disease brain. *J. Extracell. Vesicles* **11**, e12183 (2022).
5. S. Balestrini, M. A. Mikati, R. Alvarez-Garcia-Roves, M. Carboni, A. S. Hunanyan, B. Kherallah, M. McLean, L. Prange, E. De Grandis, A. Gagliardi, L. Pisciotta, M. Stagnaro, E. Veneselli, J. Campistol, C. Fons, L. Pias-Peleteiro, A. Brashear, C. Miller, R. Samoes, V. Brankovic, Q. S. Padiath, A. Potic, J. Pilch, A. Vezyroglou, A. M. E. Bye, A. M. Davis, M. M. Ryan, C. Semsarian, G. Hollingsworth, I. E. Scheffer, T. Granata, N. Nardocci, F. Ragona, A. Arzimanoglou, E. Panagiotakaki, I. Carrilho, C. Zucca, J. Novy, K. Dziezyc, M. Parowicz, M. Mazurkiewicz-Beldzinska, S. Weckhuysen, R. Pons, S. Groppa, D. S. Sinden, G. S. Pitt, A. Tinker, M. Ashworth, Z. Michalak, M. Thom, J. H. Cross, R. Vavassori, J. P. Kaski, S. M. Sisodiya, Cardiac phenotype in *ATP1A3*-related syndromes: A multicenter cohort study. *Neurology* **95**, e2866–e2879 (2020).
6. R. S. Smith, M. Florio, S. K. Akula, J. E. Neil, Y. Wang, R. S. Hill, M. Goldman, C. D. Mullally, N. Reed, L. Bello-Espinosa, L. Flores-Sarnat, F. P. Monteiro, C. B. Erasmo, E. V. F. Pinto, E. Morava, A. J. Barkovich, J. Gonzalez-Heydrich, C. A. Brownstein, S. A. McCarroll, C. A. Walsh, Early role for a Na^+, K^+-ATPase (*ATP1A3*) in brain development. *Proc. Natl. Acad. Sci. U.S.A.* **118**, e2023333118 (2021).
7. M. Mustapic, E. Eitan, J. K. Werner Jr., S. T. Berkowitz, M. P. Lazaropoulos, J. Tran, E. J. Goetzl, D. Kapogiannis, Plasma extracellular vesicles enriched for neuronal origin: A potential window into brain pathologic processes. *Front. Neurosci.* **11**, 278 (2017).
8. Y. Zhang, C. Pak, Y. Han, H. Ahlenius, Z. Zhang, S. Chanda, S. Marro, C. Patzke, C. Acuna, J. Covy, W. Xu, N. Yang, T. Danko, L. Chen, M. Wernig, T. C. Sudhof, Rapid single-step induction of functional neurons from human pluripotent stem cells. *Neuron* **78**, 785–798 (2013).
9. C.-C. Peng, D. Im, S. Sirivolu, B. Reiser, A. Nagiel, P. Neviani, L. Xu, J. L. Berry, Single vesicle analysis of aqueous humor in pediatric ocular diseases reveals eye specific CD63-dominant subpopulations. *J. Extracell. Biol.* **1**, e36 (2022).
10. N. Gebara, J. Scheel, R. Skovronova, C. Grange, L. Marozio, S. Gupta, V. Giorgione, F. Caicci, C. Benedetto, A. Khalil, B. Bussolati, Single extracellular vesicle analysis in human amniotic fluid shows evidence of phenotype alterations in preeclampsia. *J. Extracell. Vesicles* **11**, e12217 (2022).
11. Z. Ruan, D. Pathak, S. Venkatesan Kalavai, A. Yoshii-Kitahara, S. Muraoka, N. Bhatt, K. Takamatsu-Yukawa, J. Hu, Y. Wang, S. Hersh, M. Ericsson, S. Gorantla, H. E. Gendelman, R. Kayed, S. Ikezu, J. I. Luebke, T. Ikezu, Alzheimer's disease brain-derived extracellular vesicles spread tau pathology in interneurons. *Brain* **144**, 288–309 (2021).
12. G. H. Dar, C. C. Mendes, W. L. Kuan, A. A. Speciale, M. Conceicao, A. Gorgens, I. Uliyakina, M. J. Lobo, W. F. Lim, S. El Andaloussi, I. Mager, T. C. Roberts, R. A. Barker, D. C. I. Goberdhan, C. Wilson, M. J. A. Wood, GAPDH controls extracellular vesicle biogenesis and enhances the therapeutic potential of EV mediated siRNA delivery to the brain. *Nat. Commun.* **12**, 6666 (2021).
13. R. Kalluri, V. S. LeBleu, The biology, function, and biomedical applications of exosomes. *Science* **367**, (2020).
14. H. Zetterberg, Biofluid-based biomarkers for Alzheimer's disease-related pathologies: An update and synthesis of the literature. *Alzheimers Dement.* **18**, 1687–1693 (2022).
15. D. M. Rissin, C. W. Kan, T. G. Campbell, S. C. Howes, D. R. Fournier, L. Song, T. Piech, P. P. Patel, L. Chang, A. J. Rivnak, E. P. Ferrell, J. D. Randall, G. K. Provuncher, D. R. Walt, D. C. Duffy, Single-molecule enzyme-linked immunosorbent assay detects serum proteins at subfemtomolar concentrations. *Nat. Biotechnol.* **28**, 595–599 (2010).
16. J. B. Pereira, S. Janelidze, R. Ossenkoppele, H. Kvartsberg, A. Brinkmalm, N. Mattsson-Carlgren, E. Stomrud, R. Smith, H. Zetterberg, K. Blennow, O. Hansson, Untangling the association of amyloid-β and tau with synaptic and axonal loss in Alzheimer's disease. *Brain* **144**, 310–324 (2021).
17. B. Chen, L. Song, J. Yang, W. Y. Zhou, Y. Y. Cheng, Y. J. Lai, Proteomics of serum exosomes identified fibulin-1 as a novel biomarker for mild cognitive impairment. *Neural Regen. Res.* **18**, 587–593 (2023).
18. I. Arevalo-Rodriguez, N. Smailagic, M. Roque-Figuls, A. Ciapponi, E. Sanchez-Perez, A. Giannakou, O. L. Pedraza, X. Bonfill Cosp, S. Cullum, Mini-Mental State Examination (MMSE) for the early detection of dementia in people with mild cognitive impairment (MCI). *Cochrane Database Syst. Rev.* **7**, CD010783 (2021).
19. O. Pedraza, J. A. Lucas, G. E. Smith, R. C. Petersen, N. R. Graff-Radford, R. J. Ivnik, Robust and expanded norms for the Dementia Rating Scale. *Arch. Clin. Neuropsychol.* **25**, 347–358 (2010).
20. J. Simren, A. Leuzy, T. K. Karikari, A. Hye, A. L. Benedet, J. Lantero-Rodriguez, N. Mattsson-Carlgren, M. Schöll, P. Mecocci, B. Vellas, M. Tsolaki, I. Kloszewska, H. Soininen, S. Lovestone, D. Aarsland; AddNeuroMed consortium, O. Hansson, P. Rosa-Neto, E. Westman, K. Blennow, H. Zetterberg, N. J. Ashton, The diagnostic and prognostic capabilities of plasma biomarkers in Alzheimer's disease. *Alzheimers Dement.* **17**, 1145–1156 (2021).
21. C. Thery, K. W. Witwer, E. Aikawa, M. J. Alcaraz, J. D. Anderson, R. Andriantsitohaina, A. Antoniou, T. Arab, F. Archer, G. K. Atkin-Smith, D. C. Ayre, J. M. Bach, D. Bachurski, H. Baharvand, L. Balaj, S. Baldacchino, N. N. Bauer, A. A. Baxter, M. Bebawy, C. Beckham, A. Bedina Zavec, A. Benmoussa, A. C. Berardi, P. Bergese, E. Bielska, C. Blenkiron, S. Bobis-Wozowicz, E. Boilard, W. Boireau, A. Bongiovanni, F. E. Borras, S. Bosch, C. M. Boulanger, X. Breakefield, A. M. Breglio, M. A. Brennan, D. R. Brigstock, A. Brisson, M. L. Broekman, J. F. Bromberg, P. Bryl-Gorecka, S. Buch, A. H. Buck, D. Burger, S. Busatto, D. Buschmann, B. Bussolati, E. I. Buzas, J. B. Byrd, G. Camussi, D. R. Carter, S. Caruso, L. W. Chamley, Y. T. Chang, C. Chen, S. Chen, L. Cheng, A. R. Chin, A. Clayton, S. P. Clerici, A. Cocks, E. Cocucci, R. J. Coffey, A. Cordeiro-da-Silva, Y. Couch, F. A. Coumans, B. Coyle, R. Crescitelli, M. F. Criado, C. D'Souza-Schorey, S. Das, A. D. Chaudhuri, P. de Candia, E. F. De Santana, O. De Wever, H. A. Del Portillo, T. Demaret, S. Deville, A. Devitt, B. Dhondt, D. Di Vizio, L. C. Dieterich, V. Dolo, A. P. D. Rubio, M. Dominici, M. R. Dourado, T. A. Driedonks,

F. V. Duarte, H. M. Duncan, R. M. Eichenberger, K. Ekstrom, S. El Andaloussi, C. Elie-Caille, U. Erdbrugger, J. M. Falcon-Perez, F. Fatima, J. E. Fish, M. Flores-Bellver, A. Forsonits, A. Frelet-Barrand, F. Fricke, G. Fuhrmann, S. Gabrielsson, A. Gamez-Valero, C. Gardiner, K. Gartner, R. Gaudin, Y. S. Gho, B. Giebel, C. Gilbert, M. Gimona, I. Giusti, D. C. Goberdhan, A. Gorgens, S. M. Gorski, D. W. Greening, J. C. Gross, A. Gualerzi, G. N. Gupta, D. Gustafson, A. Handberg, R. A. Haraszti, P. Harrison, H. Hegyesi, A. Hendrix, A. F. Hill, F. H. Hochberg, K. F. Hoffmann, B. Holder, H. Holthofer, B. Hosseinkhani, G. Hu, Y. Huang, V. Huber, S. Hunt, A. G. Ibrahim, T. Ikezu, J. M. Inal, M. Isin, A. Ivanova, H. K. Jackson, S. Jacobsen, S. M. Jay, M. Jayachandran, G. Jenster, L. Jiang, S. M. Johnson, J. C. Jones, A. Jong, T. Jovanovic-Talisman, S. Jung, R. Kalluri, S. I. Kano, S. Kaur, Y. Kawamura, E. T. Keller, D. Khamari, E. Khomyakova, A. Khvorova, P. Kierulf, K. P. Kim, T. Kislinger, M. Klingeborn, D. J. Klinke II, M. Kornek, M. M. Kosanovic, A. F. Kovacs, E. M. Kramer-Albers, S. Krasemann, M. Krause, I. V. Kurochkin, G. D. Kusuma, S. Kuypers, S. Laitinen, S. M. Langevin, L. R. Languino, J. Lannigan, C. Lasser, L. C. Laurent, G. Lavieu, E. Lazaro-Ibanez, S. Le Lay, M. S. Lee, Y. X. F. Lee, D. S. Lemos, M. Lenassi, A. Leszczynska, I. T. Li, K. Liao, S. F. Libregts, E. Ligeti, R. Lim, S. K. Lim, A. Line, K. Linnemannstons, A. Llorente, C. A. Lombard, M. J. Lorenowicz, A. M. Lorincz, J. Lotvall, J. Lovett, M. C. Lowry, X. Loyer, Q. Lu, B. Lukomska, T. R. Lunavat, S. L. Maas, H. Malhi, A. Marcilla, J. Mariani, J. Mariscal, E. S. Martens-Uzunova, L. Martin-Jaular, M. C. Martinez, V. R. Martins, M. Mathieu, S. Mathivanan, M. Maugeri, L. K. McGinnis, M. J. McVey, D. G. Meckes Jr., K. L. Meehan, I. Mertens, V. R. Minciacchi, A. Moller, M. Moller Jorgensen, A. Morales-Kastresana, J. Morhayim, F. Mullier, M. Muraca, L. Musante, V. Mussack, D. C. Muth, K. H. Myburgh, T. Najrana, M. Nawaz, I. Nazarenko, P. Nejsum, C. Neri, T. Neri, R. Nieuwland, L. Nimrichter, J. P. Nolan, E. N. Nolte Hoen, N. Noren Hooten, L. O'Driscoll, T. O'Grady, A. O'Loghlen, T. Ochiya, M. Olivier, A. Ortiz, L. A. Ortiz, X. Osteikoetxea, O. Ostergaard, M. Ostrowski, J. Park, D. M. Pegtel, H. Peinado, F. Perut, M. W. Pfaffl, D. G. Phinney, B. C. Pieters, R. C. Pink, D. S. Pisetsky, E. Pogge von Strandmann, I. Polakovicova, I. K. Poon, B. H. Powell, I. Prada, L. Pulliam, P. Quesenberry, A. Radeghieri, R. L. Raffai, S. Raimondo, J. Rak, M. I. Ramirez, G. Raposo, M. S. Rayyan, N. Regev-Rudzki, F. L. Ricklefs, P. D. Robbins, D. D. Roberts, S. C. Rodrigues, E. Rohde, S. Rome, K. M. Rouschop, A. Rughetti, A. E. Russell, P. Saa, S. Sahoo, E. Salas-Huenuleo, C. Sanchez, J. A. Saugstad, M. J. Saul, R. M. Schiffelers, R. Schneider, T. H. Schoyen, A. Scott, E. Shahaj, S. Sharma, O. Shatnyeva, F. Shekari, G. V. Shelke, A. K. Shetty, K. Shiba, P. R. Siljander, A. M. Silva, A. Skowronek, O. L. Snyder II, R. P. Soares, B. W. Sodar, C. Soekmadji, J. Sotillo, P. D. Stahl, W. Stoorvogel, S. L. Stott, E. F. Strasser, S. Swift, H. Tahara, M. Tewari, K. Timms, S. Tiwari, R. Tixeira, M. Tkach, W. S. Toh, R. Tomasini, A. C. Torrecilhas, J. P. Tosar, V. Toxavidis, L. Urbanelli, P. Vader, B. W. van Balkom, S. G. van der Grein, J. Van Deun, M. J. van Herwijnen, K. Van Keuren-Jensen, G. van Niel, M. E. van Royen, A. J. van Wijnen, M. H. Vasconcelos, I. J. Vechetti Jr., T. D. Veit, L. J. Vella, E. Velot, F. J. Verweij, B. Vestad, J. L. Vinas, T. Visnovitz, K. V. Vukman, J. Wahlgren, D. C. Watson, M. H. Wauben, A. Weaver, J. P. Webber, V. Weber, A. M. Wehman, D. J. Weiss, J. A. Welsh, S. Wendt, A. M. Wheelock, Z. Wiener, L. Witte, J. Wolfram, A. Xagorari, P. Xander, J. Xu, X. Yan, M. Yanez-Mo, H. Yin, Y. Yuana, V. Zappulli, J. Zarubova, V. Zekas, J. Y. Zhang, Z. Zhao, L. Zheng, A. R. Zheutlin, A. M. Zickler, P. Zimmermann, A. M. Zivkovic, D. Zocco, E. K. Zuba-Surma, Minimal information for studies of extracellular vesicles 2018 (MISEV2018): A position statement of the International Society for Extracellular Vesicles and update of the MISEV2014 guidelines. *J. Extracell. Vesicles* **7**, 1535750 (2018).

22. L. J. Vella, B. J. Scicluna, L. Cheng, E. G. Bawden, C. L. Masters, C. S. Ang, N. Willamson, C. McLean, K. J. Barnham, A. F. Hill, A rigorous method to enrich for exosomes from brain tissue. *J. Extracell. Vesicles* **6**, 1348885 (2017).
23. S. Ferguson, K. S. Yang, P. Zelga, A. S. Liss, J. C. T. Carlson, C. F. Del Castillo, R. Weissleder, Single-EV analysis (sEVA) of mutated proteins allows detection of stage 1 pancreatic cancer. *Sci. Adv.* **8**, eabm3453 (2022).
24. G. R. Jun, Y. You, C. Zhu, G. Meng, J. Chung, R. Panitch, J. Hu, W. Xia; Alzheimer's Disease Genetics Consortium, D. A. Bennett, T. M. Foroud, L. S. Wang, J. L. Haines, R. Mayeux, M. A. Pericak-Vance, G. D. Schellenberg, R. Au, K. L. Lunetta, T. Ikezu, T. D. Stein, L. A. Farrer, Protein phosphatase 2A and complement component 4 are linked to the protective effect of APOE ε2 for Alzheimer's disease. *Alzheimers Dement.* **18**, 2042–2054 (2022).
25. S. Muraoka, A. M. DeLeo, M. K. Sethi, K. Yukawa-Takamatsu, Z. Yang, J. Ko, J. D. Hogan, Z. Ruan, Y. You, Y. Wang, M. Medalla, S. Ikezu, M. Chen, W. Xia, S. Gorantla, H. E. Gendelman, D. Issadore, J. Zaia, T. Ikezu, Proteomic and biological profiling of extracellular vesicles from Alzheimer's disease human brain tissues. *Alzheimers Dement.* **16**, 896–907 (2020).
26. S. Muraoka, A. M. DeLeo, Z. Yang, H. Tatebe, K. Yukawa-Takamatsu, S. Ikezu, T. Tokuda, D. Issadore, R. A. Stern, T. Ikezu, Proteomic Profiling of Extracellular Vesicles Separated from Plasma of Former National Football League Players at Risk for Chronic Traumatic Encephalopathy. *Aging Dis.* **12**, 1363–1375 (2021).
27. Y. You, K. Borgmann, V. V. Edara, S. Stacy, A. Ghorpade, T. Ikezu, Activated human astrocyte-derived extracellular vesicles modulate neuronal uptake, differentiation and firing. *J. Extracell. Vesicles* **9**, 1706801 (2020).
28. J. Chen, E. E. Bardes, B. J. Aronow, A. G. Jegga, ToppGene Suite for gene list enrichment analysis and candidate gene prioritization. *Nucleic Acids Res.* **37**, W305–W311 (2009).

Acknowledgments: We would like to thank the staff members (C. Scholes, B. C. Melvin, and S. D. Mann Jr.) of the Laboratory of Molecular NeuroTherapeutics, M. L. Ushman and M. Russo at Mayo Clinic for technical assistances, NIH NeuroBioBank for unfixed human frozen brain tissues, R. Rissman from the University of California, San Diego for plasma samples, and NanoView Biosciences for the SP-IRIS analysis and imaging. We also thank BioRender.com for providing resources and templates for the illustrations. **Funding:** This work is funded by Florida Department of Health Ed and Ethel Moore Alzheimer's Disease Research Program-22A04 (Y.Y.), Alzheimer's Association AARF-22-918114 (Y.Y.), Cure Alzheimer's Fund (T.I. and S.I.), NIH RF1 AG054199 (T.I.), R01AG054672 (T.I.), R01 AG066429 (T.I.), R01 AG067763 (T.I.), R01 AG072719 (T.I.), R01 AG079859 (S.I.), and RF1 AG082704 (S.I. and T.I.). **Author contributions:** Y.Y., Z.Z., and T.I. designed research; Y.Y., Z.Z., N.S., M.E., M.S., and Y.A.M. carried out experiments; Y.Y., Z.Z., M.S., and Y.A.M. analyzed data; S.I. and T.K. provided the oversight and suggestion on data interpretation; S.A.S. provided advice on mass spectrometry; Y.Y. and Z.Z. wrote the manuscript with input from co-authors; T.I. supervised the study and contributed to manuscript preparation and editing. All authors have read and approved the final version of the manuscript. **Competing interests:** T.I., Y.Y., and Z.Z. have filed a New Technology Disclosure with Mayo Clinic Venture relating to the identification and use of ATP1A3 for NDEV isolation. M.S. is an employee of Nanoview Biosciences Inc. Y.A.M. is currently an employee of SciNeuro Pharmaceuticals Inc. and consults Kisbee Thereapeutics. N.S. is currently an employee of Abbvie Inc. T.I. consults Takeda. The authors declare that they have no other competing interests. **Data and materials availability:** All data needed to evaluate the conclusions in the paper are present in the paper and/or the Supplementary Materials. Source data are provided with this paper. The human plasma samples can be provided by R. Rissman at University of California, San Diego pending scientific review and completed material transfer agreement. Request for the human plasma samples should be made to R. Rissman (rrissman@health.ucsd.edu).

Submitted 21 April 2023
Accepted 15 August 2023
Published 15 September 2023
10.1126/sciadv.adi3647